

## **Title**

**Measurements of carbonic anhydrase activity *in vivo* using hyperpolarized  $^{13}\text{C}$ -magnetic resonance spectroscopy demonstrate its importance in pH regulation.**

## **Authors**

Ferdia A. Gallagher<sup>1,2</sup>, Helen Sladen<sup>1</sup>, Mikko I. Kettunen<sup>1</sup>, Eva M. Serrao<sup>1</sup>, Tiago B. Rodrigues<sup>1</sup>, Alan Wright<sup>1</sup>, Andrew Gill<sup>2</sup>, Sarah McGuire<sup>1</sup>, Thomas C. Booth<sup>1</sup>, Joan Boren<sup>1</sup>, Alan McIntyre<sup>3</sup>, Jodi L. Miller<sup>1</sup>, Shen-Han Lee<sup>1</sup>, Davina Honess<sup>1</sup>, Sam E. Day<sup>1</sup>, De-en Hu<sup>1</sup>, William J. Howat<sup>1</sup>, Adrian L. Harris<sup>3</sup>, Kevin M. Brindle<sup>1</sup>.

## **Affiliations**

1. Cancer Research UK Cambridge Institute, University of Cambridge, Li Ka Shing Centre, Robinson Way, Cambridge CB2 0RE, UK.
2. Department of Radiology, University of Cambridge, Box 218 Level 5, Addenbrooke's Hospital, Cambridge CB2 0QQ, UK.
3. Weatherall Institute of Molecular Medicine, University of Oxford, John Radcliffe Hospital, Headington, Oxford, OX3 9DS, UK.

## **Conflicts of interest:**

FAG and KMB have research support from GE Healthcare. The authors declare no other conflicts of interest.

## **Keywords**

Carbonic anhydrase

Tumor pH

Bicarbonate

Hyperpolarized carbon

Dynamic nuclear polarization

## **Running Title**

Probing carbonic anhydrase with hyperpolarized carbon-13 MRS

## Abstract

Carbonic anhydrase (CA) buffers tissue pH by catalyzing the rapid interconversion of carbon dioxide ( $\text{CO}_2$ ) and bicarbonate ( $\text{HCO}_3^-$ ). We assessed the functional activity of CAIX in two colorectal tumor models, expressing different levels of the enzyme, by measuring the rate of exchange of hyperpolarized  $^{13}\text{C}$  label between bicarbonate ( $\text{H}^{13}\text{CO}_3^-$ ) and carbon dioxide ( $^{13}\text{CO}_2$ ), following injection of hyperpolarized  $\text{H}^{13}\text{CO}_3^-$ , using  $^{13}\text{C}$  magnetic resonance spectroscopy ( $^{13}\text{C}$ -MRS) magnetization transfer measurements.  $^{31}\text{P}$ -MRS measurements of the chemical shift of the pH probe, 3-aminopropylphosphonate, and  $^{13}\text{C}$ -MRS measurements of the  $\text{H}^{13}\text{CO}_3^-/^{13}\text{CO}_2$  peak intensity ratio showed that CAIX overexpression lowered extracellular pH in these tumors. However, the  $^{13}\text{C}$  measurements overestimated pH due to incomplete equilibration of the hyperpolarized  $^{13}\text{C}$  label between the  $\text{H}^{13}\text{CO}_3^-$  and  $^{13}\text{CO}_2$  pools. Paradoxically, tumors overexpressing CAIX showed lower enzyme activity using magnetization transfer measurements, which can be explained by the more acidic extracellular pH in these tumors and the decreased activity of the enzyme at low pH. This explanation was confirmed by administration of bicarbonate in the drinking water, which elevates tumor extracellular pH and restored enzyme activity to control levels. These results suggest that CAIX expression is increased in hypoxia to compensate for the decrease in its activity produced by a low extracellular pH, and supports the hypothesis that a major function of CAIX is to lower the extracellular pH.

## **Introduction**

Carbonic anhydrase (CA) catalyzes the rapid interconversion of carbon dioxide ( $\text{CO}_2$ ) and bicarbonate ( $\text{HCO}_3^-$ ) and forms an essential part of the major physiological buffering system in tissues. The enzyme is highly conserved, forming a large family of isoforms, which are both cytosolic and membrane-bound. CA plays a major role in pH buffering and aids the transmembrane diffusion of both cellular protons ( $\text{H}^+$ ) and  $\text{CO}_2$  (1). The acidic extracellular tumor environment is generated by both lactate accumulation derived from glycolysis (2), and glycolysis-independent pathways such as the formation of  $\text{CO}_2$  (3). There are two main mechanisms for removing the intracellular acid generated by these pathways into the extracellular space:  $\text{HCO}_3^-$ -independent mechanisms involving  $\text{H}^+$  transporters such as  $\text{Na}^+/\text{H}^+$  or  $\text{H}^+/\text{lactate}$  exchange; and  $\text{HCO}_3^-$ -dependent mechanisms where intracellular  $\text{H}^+$  is buffered by  $\text{HCO}_3^-$  imported by transporters such as the  $\text{Na}^+/\text{HCO}_3^-$  co-transporter (1). The latter are affected by the slow kinetics of  $\text{CO}_2$  hydration and dehydration and therefore upregulation of CA activity may alter pH regulation.

The expression of a membrane-bound isoform of the enzyme - carbonic anhydrase 9 or CAIX - is upregulated in hypoxic tissues by the transcription factor hypoxia inducible factor-1 alpha ( $\text{HIF-1}\alpha$ ) (4). In tumors, CAIX expression has been shown to correlate with a poor prognosis, a more malignant phenotype and increased invasiveness (5). The expression of CAIX has previously been imaged using an  $^{124}\text{I}$ -labelled antibody and Positron Emission Tomography (PET) in patients with renal carcinoma (6); however, this method measures only the concentration of the enzyme and not its activity. Moreover, there are other isoforms of CA, which are also upregulated in tumors e.g CAXII (5), which will not be detected by probes that are specific for CAIX. The activity of the enzyme is dependent on several factors within the

tumor microenvironment, which may alter *ex vivo*; therefore an accurate estimate of the activity of the enzyme from measurements on excised tissue is difficult, requiring measurements to be made *in vivo*.

Dynamic nuclear polarization (DNP) can increase the sensitivity of magnetic resonance spectroscopy (MRS) by more than four orders of magnitude. Application of the technique to  $^{13}\text{C}$ -labelled metabolites (7) has allowed the spatial distribution of the injected molecules and the products formed from them to be imaged non-invasively *in vivo* (reviewed in (8-10)).  $^{13}\text{C}$ -labelled bicarbonate ( $\text{H}^{13}\text{CO}_3^-$ ) has been polarized using DNP and following intravenous injection into an animal the spatial distribution of both the injected  $\text{H}^{13}\text{CO}_3^-$  and the  $^{13}\text{C}$ -labelled carbon dioxide ( $^{13}\text{CO}_2$ ) produced from it were imaged (11). Since CA catalyzes rapid exchange between bicarbonate and carbon dioxide, the ratio of the signals from the two molecules can be used to image tissue pH, provided that the reaction reaches isotopic equilibrium (11,12). This was shown to be the case in a murine lymphoma model, where the pH estimated from the  $\text{H}^{13}\text{CO}_3^-/^{13}\text{CO}_2$  ratio showed good agreement with the extracellular pH estimated from the chemical shift of the 3-aminopropylphosphonate (3-APP) resonance in  $^{31}\text{P}$ -MR spectra. The measured pH was dominated by the extracellular component due to the relatively high concentration of bicarbonate in the extracellular space compared to the intracellular space, as well as the relatively slow diffusion and transport of hyperpolarized  $^{13}\text{CO}_2$  and  $\text{H}^{13}\text{CO}_3^-$  across the plasma membrane, when compared to the lifetime of the polarization (11,12). The technique can also be used to estimate the activity of CA *in situ* by measuring the rate of magnetization transfer between the hyperpolarized  $\text{H}^{13}\text{CO}_3^-$  and  $^{13}\text{CO}_2$  resonances. This can be determined in a saturation transfer experiment from the decrease in the  $\text{H}^{13}\text{CO}_3^-$  peak intensity following selective saturation of the  $^{13}\text{CO}_2$  peak (11). These

measurements therefore provide a means to investigate the role of CA upregulation in proton transport across the plasma membrane.

We show here, using  $^{13}\text{C}$ -MRS magnetisation transfer measurements, that there is a disparity between the level of CAIX expression and  $^{13}\text{C}$ -MRS measurements of CA activity, where the lower CA activity measured in tumors overexpressing CAIX can be explained by the lower extracellular tumor pH and a consequent reduction in the specific activity of the enzyme.

## **Materials and methods**

### **Hyperpolarized $\text{H}^{13}\text{CO}_3^-$ production and polarization**

$^{13}\text{C}$ -labelled cesium bicarbonate ( $\text{CsH}^{13}\text{CO}_3$ ) was made by slowly adding  $^{13}\text{CO}_2$  (Sigma-Aldrich, UK) to an evacuated flask containing 0.36 M CsOH hydrate (Sigma-Aldrich, UK) until the pH reached  $\sim 7.3$ , when the sample was then lyophilized.  $\text{CsH}^{13}\text{CO}_3$  (0.70 mmol) was dissolved in 63.3  $\mu\text{l}$  of water and 0.54 mmol of glycerol (Sigma-Aldrich, UK); 2.0  $\mu\text{mol}$  of a free radical (OX063, GE Healthcare, UK) and 141 nmol of gadolinium were added. The gadolinium was added as either a univalent chelate for the *in vivo* experiments (gadoteric acid with a single gadolinium atom per molecule of chelate, Guerbet, France) or a trivalent chelate for the *in vitro* experiments (Gd-3, with three gadolinium atoms per molecule of chelate, GE Healthcare, Amersham, UK); the final concentration of gadolinium was constant in both preparations. Aliquots (10  $\mu\text{l}$ ) were dropped into liquid nitrogen to form pellets, which were placed in a Hypersense polarizer (Oxford Instruments, Abingdon, UK). The  $\text{CsH}^{13}\text{CO}_3$  was polarized using a method similar to that described previously (11) with a microwave source at  $\sim 94$  GHz. The frozen sample was dissolved using 6 ml of an 80 mM phosphate buffer at pH

7.5 containing 100 mg/l diaminoethanetetraacetic acid (EDTA) heated to  $\sim 180^{\circ}\text{C}$  and pressurized to 10 bar. The concentration and temperature of  $\text{H}^{13}\text{CO}_3^-$  in the final solution was  $\sim 100$  mM and  $\sim 37^{\circ}\text{C}$  respectively. Polarization was measured using a polarimeter (Oxford Instruments, UK).

### **Measurements of CA activity *in vitro***

A phantom containing 5 tubes was used, each containing 0.4 ml of a 500 mM phosphate buffer and 100 mg/l diaminoethanetetraacetic acid (EDTA) at pH 7.4; to each was added varying concentrations of CA (2532 units/mg; C3934, Sigma Aldrich, UK), from 0-8  $\mu\text{g/ml}$ . Imaging of the tubes was performed in a 9.4 T vertical wide-bore magnet (Oxford Instruments, Oxford, UK). Transverse  $^1\text{H}$ -MR images were acquired using a quadrature  $^1\text{H}$ -tuned volume coil (Agilent, USA).  $^{13}\text{C}$ -MRS images were acquired using a  $^{13}\text{C}$ -tuned surface coil placed adjacent to the tubes: 300  $\mu\text{l}$  of  $\sim 100$  mM hyperpolarized  $\text{CsH}^{13}\text{CO}_3$  was injected simultaneously into each tube and a series of non-slice selective echo-planar  $^{13}\text{C}$  images (EPI) of the  $\text{H}^{13}\text{CO}_3^-$  resonance were acquired using: a nominal flip angle of  $10^{\circ}$ ; TR = 100 ms; TE = 1.6 ms; data matrix 48 x 32 collected in two segments; field-of-view 64 x 32 mm. Between image acquisitions, the  $^{13}\text{CO}_2$  resonance was selectively saturated for a total of 670 ms with a nominal  $B_1$  field of 100 Hz. A CA activity map was derived by dividing the  $\text{H}^{13}\text{CO}_3^-$  signal intensity in the first image by that in the last image, and displaying the resulting image intensity on a gray scale. To reduce noise in the final image, pixels in the ratio image were set to black if the voxels used to create the ratio showed a  $\text{H}^{13}\text{CO}_3^-$  signal intensity that was less than 5% of the maximum  $\text{H}^{13}\text{CO}_3^-$  signal intensity. Mean signal intensities in each tube were measured by

averaging the  $\text{H}^{13}\text{CO}_3^-$  signal in the voxels within each tube, where the position of these was determined from the  $^1\text{H}$ -MR image. This average signal in the first and last  $\text{H}^{13}\text{CO}_3^-$  images was used to calculate the rate of decrease in the natural logarithm of the  $\text{H}^{13}\text{CO}_3^-$  signal intensity in each tube, which was plotted against the respective CA concentration in each tube and a correlation co-efficient was calculated (Excel, Microsoft, USA).

### **CAIX overexpressing cells**

HCT116 cells were grown in RPMI medium supplemented with 10% FBS (Invitrogen, UK) at 5%  $\text{CO}_2$  and  $37^\circ\text{C}$ . A human *CA9* cDNA construct was used to generate a stable cell line (CA9/1), together with an empty vector control cell line (EV5) as described previously (13). Cell lines were transfected with FuGENE 6 (Roche, UK) and grown under selective pressure with G418 (Invitrogen, UK) at 0.4 mg/ml until no mock-transfected cells remained. Individual clones were isolated using cloning cylinders (Sigma, UK).

### **CAIX Western blot**

Protein extracts were prepared from cells by homogenization under denaturing conditions using a radioimmunoprecipitation assay buffer (RIPA) and protease inhibition (Halt protease inhibitor, Thermo Fisher Scientific, UK). Aliquots containing 30  $\mu\text{g}$  protein were separated by SDS-PAGE (Thermo Fisher Scientific, UK). Following membrane transfer and overnight blocking, CAIX was detected using a 1:50 dilution of a rabbit monoclonal anti-human CAIX antibody (Abcam, UK). Actin, which was used as a loading control, was detected using a goat monoclonal anti-human beta-actin antibody (Abcam, UK) at a dilution of 1:10,000. The membrane was washed 4 times for 5 min in tris-buffered saline at pH 7.6 with 0.1% Tween 20



(TBST) before adding a donkey anti-rabbit-800CW secondary antibody at a 1:5,000 dilution and a donkey anti-goat-680LT secondary antibody at a 1:10,000 dilution (Li-Cor Biosciences, USA) for 45 min at room temperature. Following three 5 min washes in TBST and one in tris-buffered saline (TBS), the membrane was scanned using a Li-Cor Odyssey system (Li-Cor Biosciences, USA) using the green 800 channel for CAIX and the red 700 channel for beta-actin. All antibodies were diluted in blocking buffer (Odyssey, Li-Cor Biosciences, USA) containing 0.1% Tween.

### **Measurements of carbonic anhydrase activity *in vitro***

The CO<sub>2</sub> hydration time constant, which was used as a surrogate of CA activity, was determined from the time taken for a cell suspension to decrease by one pH unit following the addition of a saturated CO<sub>2</sub> solution. The saturated solution was prepared by bubbling gaseous CO<sub>2</sub> (BOC, UK) through a water-filled gas burette submerged in ice. Cells, 9 x 10<sup>7</sup> CA9/1 or EV5, were harvested, washed and resuspended in 3 ml of PBS at 4°C on ice. A further 3 ml of the saturated CO<sub>2</sub> solution was added and the pH changes were recorded continuously over time. The time, to the nearest second, for the pH of the cell suspension to drop one unit was corrected for protein content measured using a Bradford assay, averaged for each cell line, and the reciprocal of this value (in s<sup>-1</sup> mg protein<sup>-1</sup>) was recorded. This was repeated for lysed cell samples, in which the cells had been freeze-thaw lysed by two cycles of immersion in liquid nitrogen and warming in a 37°C water bath.

### **Tumor implantation**

All experiments were conducted in compliance with project and personal licenses issued under the Animals (Scientific Procedures) Act of 1986. Protocols were approved by the Cancer

Research UK, Cambridge Institute Animal Welfare and Ethical Review Body. Xenografts were grown by subcutaneous implantation of  $1 \times 10^7$  cells, in 100  $\mu\text{l}$  of PBS, into the flanks of male NOD SCID gamma (NSG) mice. Tumors were grown from both cells overexpressing CAIX (CA9/1) and cells transfected with the empty vector (EV5) for between 20 and 24 days after implantation. Imaging was performed when the tumors had grown to approximately  $2 \text{ cm}^3$ . Tumors produced from the two cell lines grew at approximately the same rate. Bicarbonate treated animals were given 200 mM sodium bicarbonate solution *ad libitum* instead of water for 5-7 days prior to imaging, which has been shown previously to elevate tumor extracellular pH (14).

Animals were anaesthetized by inhalation of 1-3% isoflurane (Isoflo, Abbotts Laboratories Ltd, UK) in a mixture of 25% medical oxygen and 75% air. Breathing rate and body temperature were monitored continuously and temperature was maintained using a current of warm air through the bore of the magnet.

### ***In vivo* $^{13}\text{C}$ -magnetic resonance spectroscopy**

$^{13}\text{C}$ -MRS was performed using a 7 T horizontal bore magnet (Agilent, USA) and an actively decoupled dual-tuned  $^{13}\text{C}$ - $^1\text{H}$  volume transmit coil (Rapid Biomedical, Germany) with a 20 mm diameter  $^{13}\text{C}$ -tuned surface receive coil (Rapid Biomedical, Germany) placed over the tumor.

Tumor localization was determined using  $^1\text{H}$  spin-echo imaging: field-of-view: 32 x 32 mm; data matrix 128 x 128; TR = 1.8 s; TE = 20 ms; slice thickness 2 mm. For dynamic  $^{13}\text{C}$ -MRS, a 6 mm oblique coronal slice through the tumor was chosen to avoid inclusion of other tissues

and slice-selective shimming was performed. Following this, 0.2 ml of ~100 mM hyperpolarized  $\text{CsH}^{13}\text{CO}_3$  dissolved in  $\text{D}_2\text{O}$  was injected intravenously into a tail vein outside the magnet and the animal was then replaced inside the magnet; imaging was commenced ~ 7 s after the start of the injection. A dynamic series of  $^{13}\text{C}$  spectra were acquired through the tumor: spectral width 8 kHz; 4721 complex points; TR = 1 s; TE = 1.8 ms. The first two  $^{13}\text{C}$  spectra were excluded from the analysis to allow the injected bicarbonate to reach a steady state in the tissue. The second two  $^{13}\text{C}$  spectra were acquired following a control irradiation using a spectrally selective 100 ms pulse with a nominal  $B_1$  field of 100 Hz at 197 ppm, which is 36 ppm downfield from the  $\text{H}^{13}\text{CO}_3^-$  resonance and equal to the frequency difference between the  $\text{H}^{13}\text{CO}_3^-$  resonance and the upfield  $^{13}\text{CO}_2$  resonance. The second of these spectra was used to normalize the subsequent data. A further 5 spectra were acquired following saturation of the  $^{13}\text{CO}_2$  resonance at 125 ppm. The first order rate constant describing label flux between  $\text{H}^{13}\text{CO}_3^-$  and  $^{13}\text{CO}_2$  was estimated from a log plot of the hyperpolarized  $\text{H}^{13}\text{CO}_3^-$  signal intensity versus time.

***In vivo*  $^{31}\text{P}$ -magnetic resonance spectroscopy and dynamic contrast enhanced (DCE) MRI.**

In a separate group of ten animals (five EV5 and five CA9/1 tumor-bearing animals),  $^{31}\text{P}$ -MRS spectra were acquired using a 9.4 T horizontal bore magnet (Agilent, USA) and a 25 mm diameter  $^{31}\text{P}$ -tuned surface coil (Agilent, USA) placed over the tumor. An intraperitoneal injection of 0.3 ml of a 64 mg/ml solution of 3-APP in phosphate-buffered saline was administered 15 min before spectral acquisition, as described previously (11,15).

An ISIS pulse sequence with a 90° BIR-4 excitation pulse was used for acquiring  $^{31}\text{P}$  spectra from a voxel that enclosed the entire subcutaneous tumor (TR = 3 s, 8k points and 12019 Hz sweep width). The  $^{31}\text{P}$  spectra were acquired as 4 pairs of 128 averages with one spectrum of each pair acquired with a central frequency at +2 ppm and the other at +24 ppm with respect to phosphocreatine at 0 ppm. Using pairs of acquisitions gave improved signal-to-noise for the adenosine triphosphate (ATP) and phosphomonoester resonances in one spectrum and 3-APP in the other. After Fourier transformation, each spectral-pair was referenced to the mean chemical shift of all three ATP resonances and the spectra were summed to give a combined spectrum for chemical shift analysis. The pH was calculated from the whole tumor spectrum by measuring the chemical shift difference between the 3-APP resonance and the  $\gamma$ -ATP peak, similar to methods described previously (11,15).

DCE-MRI was performed in six animals (three EV5 and three CA9/1 tumor-bearing animals) at 7 T using a  $^1\text{H}$  volume coil (Rapid Biomedical, Germany). Fast inversion-recovery gradient-echo images were acquired at 7 different inversion-recovery times (100 – 10000 ms) prior to injection of contrast agent. These allowed calculation of native  $T_1$  maps using pixel-by-pixel three parameter non-linear fitting to a monoexponential function. Fat-saturated  $T_1$ -weighted images were acquired dynamically before, during and after intravenous injection of 0.2 mmol/kg gadopentetate dimeglumine (Magnevist®, Bayer, UK). The gadolinium chelate concentrations were estimated from image signal enhancement, using  $T_1$  values calculated from the native  $T_1$  maps (16,17). Regions of interest were drawn around each tumor and the tumor-containing pixels were analyzed for the initial area under the contrast agent uptake curve during the first 180 s (IAUGC180) after the arrival of the bolus of contrast agent. Pixels with a

numerical value of zero or below were rejected and the median value for the remaining pixels within each tumor was calculated.

### **Histology and immunohistochemistry**

Following imaging, the tumors from sacrificed mice were excised, fixed in formalin and paraffin-embedded as standard. Sections of 3  $\mu\text{m}$  thickness were stained with hemotoxylin and eosin using a Leica ST5020 Multistainer (Leica Biosystems, UK). Immunohistochemistry (IHC) was performed on adjacent sections using the fully automated Leica Bond III (Leica Biosystems, Milton Keynes, UK) and the Polymer Refine Detection System (CAIX) and Intense R Detection System (CD31) with Diaminobenzidine (DAB) Enhancer (Leica Biosystems, UK). Endogenous peroxidase was blocked with a 3% peroxide solution for 5 min and sections were counterstained with haematoxylin (Leica Biosystems, UK). Washing between each step was undertaken with Leica Bond Wash (Leica Biosystems, UK).

CAIX was detected using a 1:100 dilution of a mouse monoclonal anti-human CAIX antibody (Clone M75, BioScience, Slovakia) for 15 minutes (13); this antibody recognizes the proteoglycan domain and is therefore specific for intact CAIX. Heat-induced antigen retrieval was performed with sodium citrate at pH 6 (Leica Biosystems, UK) for 20 minutes at 100°C. Staining for CD31 was achieved using a monoclonal rat anti-mouse antibody (Clone MEC13.3, BD Biosciences, UK) at a 1:100 dilution with a biotinylated donkey anti-rat secondary (Jackson ImmunoResearch, USA) at a 1:250 dilution. Epitope retrieval was performed with a proteinase k enzyme digestion (Leica Biosystems, UK), diluted 1:167 and incubated at 37°C for 10 min. Post IHC, dehydration and clearing was performed using a Leica ST5020 Multistainer (Leica Biosystems, UK) and mounting using a Leica CV5030 automated system

(Leica Biosystems, UK). CD31 staining was digitized using an Aperio system (Leica, UK) and tumor microvessel density calculated using the Microvessel Analysis V1.0 software from Aperio using the average of thirty representative 1 x 1 mm regions placed within the tumor section on each slide.

## **Results**

$\text{H}^{13}\text{CO}_3^-$  and  $^{13}\text{CO}_2$  are in rapid exchange in the reaction catalyzed by CA:



where  $k_1$  and  $k_2$  are first order rate constants. Exchange of hyperpolarized  $^{13}\text{C}$  label between  $\text{H}^{13}\text{CO}_3^-$  and  $^{13}\text{CO}_2$  can be described by equation (2):

$$d(\text{H}^{13}\text{CO}_3^-)_Z / dt = -r((\text{H}^{13}\text{CO}_3^-)_Z - (\text{H}^{13}\text{CO}_3^-)_{\text{eq}}) - k_1(\text{H}^{13}\text{CO}_3^-)_Z + k_2(^{13}\text{CO}_2)_Z \quad (2)$$

where  $(\text{H}^{13}\text{CO}_3^-)_Z$  and  $(^{13}\text{CO}_2)_Z$  represent the polarizations of the  $^{13}\text{C}$  nucleus in these two species,  $(\text{H}^{13}\text{CO}_3^-)_{\text{eq}}$  represents the bicarbonate  $^{13}\text{C}$  polarization at equilibrium (time  $\rightarrow \infty$ ) and  $\rho$  is its spin lattice relaxation rate. In a hyperpolarized experiment  $(\text{H}^{13}\text{CO}_3^-)_Z \gg (\text{H}^{13}\text{CO}_3^-)_{\text{eq}}$  and, following saturation of the  $^{13}\text{CO}_2$  resonance,  $(^{13}\text{CO}_2)_Z \sim 0$ . Therefore equation 2 reduces to:

$$d(\text{H}^{13}\text{CO}_3^-)_Z / dt = -(r + k_1)(\text{H}^{13}\text{CO}_3^-)_Z \quad (3)$$

which, following integration, gives:

$$\ln \frac{\hat{c}(\text{H}^{13}\text{CO}_3^-)}{\hat{c}(\text{H}^{13}\text{CO}_3^-)_0} = -(r + k_1)t \quad (4)$$

where  $(\text{H}^{13}\text{CO}_3^-)_0$  is the bicarbonate  $^{13}\text{C}$  polarization at  $t = 0$ . Therefore a plot of the natural logarithm of the  $\text{H}^{13}\text{CO}_3^-$  signal following saturation of the  $^{13}\text{CO}_2$  resonance has a slope of  $-(r + k_1)$ , which is proportional to CA activity.

### **Magnetization transfer measurements of CA activity *in vitro***

$^{13}\text{C}$ -labelled cesium bicarbonate was hyperpolarized to 17%, which represents a 20,000-fold increase above thermal polarization at 37 °C and 9.4 T (Figure 1A). After saturation of the  $^{13}\text{CO}_2$  resonance, the tubes with the most CA activity showed the greatest decrease in  $\text{H}^{13}\text{CO}_3^-$  signal (Figure 1B). The ratio image derived from the first and last echo-planar images showed that the signal intensity in each tube correlated with the amount of CA present; the higher the CA concentration, the greater the decrease in the  $\text{H}^{13}\text{CO}_3^-$  signal and therefore the brighter the ratio image (Figure 1C). The slope of a plot of the natural logarithm of the  $\text{H}^{13}\text{CO}_3^-$  signal versus time showed a good correlation with the CA concentration (correlation coefficient  $R^2 = 0.98$ ; Figure 1D).

### **CAIX expression and functional activity in cells**

Western blots demonstrated low endogenous CAIX expression in the wild type HCT116 cell line, which was increased in cells that had been transfected with a vector expressing CAIX (CA9/1), but not in cells transfected with the empty vector (EV5; Figure 2). A faint additional

band, approximately 2 kDa heavier than the main CAIX band, was also identified, as reported previously with this antibody (18).

Functional overexpression of CAIX was determined by measuring the hydration time constant for dissolved carbon dioxide, which is the reciprocal of the time for a cell suspension to lower the pH by 1 unit following addition of a saturated CO<sub>2</sub> solution. This was  $0.013 \pm 0.002 \text{ s}^{-1} \text{ mg protein}^{-1}$  (SEM; n = 10) for CA9/1 cells and  $0.005 \pm 0.000$  (SEM; n = 10) for EV5 cells ( $p < 0.005$ ). There was an increase in CA activity following lysis of EV5 cells ( $p < 0.005$ ) and a smaller increase in CA9/1 cells ( $p = 0.15$ ; Figure 3), demonstrating that the majority of CA activity in CA9/1 cells was extracellular. The intracellular component of CA activity, derived from the difference between the total lysed measurement and the whole cell (or extracellular) measurement, was similar in both cell lines, at approximately  $0.005 \text{ s}^{-1} \text{ mg protein}^{-1}$ .

#### **CAIX expression and magnetization transfer measurements of enzyme activity in tumors**

Overexpression of CAIX in CA9/1 tumors was demonstrated by staining tumor sections with an anti-CAIX antibody (Figure 4). There was considerably more staining in CA9/1 tumors when compared to wild-type and EV5 tumors. In the EV5 and wild-type HCT116 tumors, CAIX expression was heterogeneous and circumferential in distribution compared to the more homogeneously distributed CAIX expression in the CA9/1 tumors.

Following tail vein injection of hyperpolarized  $\text{H}^{13}\text{CO}_3^-$ ,  $\text{H}^{13}\text{CO}_3^-$  and  $^{13}\text{CO}_2$  resonances were observed in  $^{13}\text{C}$ -MR spectra of the tumors (Figure 5A). Normalized log plots of the bicarbonate signal intensity, following saturation of the  $^{13}\text{CO}_2$  resonance, showed a significantly slower rate of decay in CA9/1 tumors ( $-0.23 \pm 0.01 \text{ s}^{-1}$ ; n = 6) when compared to EV5 tumors ( $-0.26 \pm$



0.01 s<sup>-1</sup>; n = 6; p = 0.02), despite higher levels of CAIX expression (Figure 5B). In a separate group of animals with CA9/1 tumors, which were administered with oral bicarbonate to elevate tumor pH, the decay of the H<sup>13</sup>CO<sub>3</sub><sup>-</sup> signal was accelerated such that the curve resembled that seen with the EV5 tumors; the initial slope of this curve was -0.23 ± 0.03 s<sup>-1</sup> (n = 5; p = 0.09; Figure 5B).

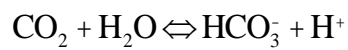
Tumor extracellular pH was estimated in two ways: firstly from the ratio of the H<sup>13</sup>CO<sub>3</sub><sup>-</sup> and <sup>13</sup>CO<sub>2</sub> signal intensities and secondly from the chemical shift of the 3-APP resonance in <sup>31</sup>P-MR spectra of tumors in animals injected i.p. with 3-APP. The pH was calculated from the <sup>13</sup>C spectra using the Henderson-Hasselbalch equation and assuming that the pKa was 6.1 and that there had been full isotopic equilibration (19). The apparent pH was 7.77 ± 0.24 (SEM; n=6) for EV5 tumors and 7.56 ± 0.07 for CA9/1 tumors (SEM; n=6), which rose to 7.71 ± 0.15 in CA9/1 tumors in animals treated with oral bicarbonate (SEM; n=5). In some experiments, the H<sup>13</sup>CO<sub>3</sub><sup>-</sup> resonance was split, with two peaks approximately 1 ppm apart (Figure 5C), which varied in their relative intensities. Following saturation of the <sup>13</sup>CO<sub>2</sub> resonance, only the downfield peak decreased in intensity, showing that that the upfield peak was not in rapid exchange with the <sup>13</sup>CO<sub>2</sub> pool. When present, the non-exchanging peak was excluded from the analysis as it does not contribute to the measured pH and inclusion would have created further disparity between the <sup>31</sup>P and <sup>13</sup>C measures of pH. The extracellular pH was calculated in a different group of animals using <sup>31</sup>P-MRS. This was 6.81 ± 0.05 (SEM; n=5) for EV5 and 6.66 ± 0.12 (SEM; n=5) for CA9/1 tumors.

There was no significant difference between the two tumor types in either the microvessel density, estimated from CD31 immunohistochemistry, or tumor perfusion, estimated using

DCE-MRI. There were  $2.65 \pm 0.60 \times 10^{-5}$  vessels per  $\mu\text{m}^2$  (average  $\pm$  S.D;  $n = 4$ ) in the CA9/1 tumors and an area under the contrast agent uptake curve (IAUGC180) of  $6.6 \pm 1.6$  mM s (mean  $\pm$  S.D.;  $n = 3$ ) and  $2.83 \pm 0.42 \times 10^{-5}$  vessels per  $\mu\text{m}^2$  ( $n = 3$ ) in the EV5 tumors and an IAUGC180 of  $12.1 \pm 3.2$  mM s ( $n = 3$ ).

## **Discussion**

Many pathological states are characterized by an acidic extracellular pH; in tumors this has been attributed to poor perfusion, increased lactic acid and  $\text{CO}_2$  production, as well as alterations in buffering capacity (20,21). Bicarbonate acts as one of the main biological buffers *in vivo*. CA catalyzes the reaction:



and therefore facilitates shuttling of protons out of the cell. Intracellular  $\text{CO}_2$  diffuses across the plasma membrane, where it rapidly forms extracellular  $\text{HCO}_3^-$  and a proton, which lowers the extracellular pH; the  $\text{HCO}_3^-$  is then transported back inside the cell (1). This is essential for the process to continue and can generate  $\text{CO}_2$  independently of oxidative phosphorylation.

We have shown previously, in a murine lymphoma model, that the ratio of the signals from injected hyperpolarized  $\text{H}^{13}\text{CO}_3^-$ , and the  $^{13}\text{CO}_2$  formed from it, could be used to estimate tumor extracellular pH. The pH determined in this way showed good agreement with that estimated from  $^{31}\text{P}$ -MRS measurements of the chemical shift of an extracellular pH probe, 3-APP (11,12). In contrast, in the implanted tumors derived from the two colorectal cancer cell lines used here, the tumor pH calculated from the hyperpolarized  $\text{H}^{13}\text{CO}_3^-/^{13}\text{CO}_2$  signal intensity ratio was higher than that measured using  $^{31}\text{P}$ -MRS and greater than that normally

found in the extracellular space in tumors (20). Moreover, the extracellular pHs measured here using  $^{31}\text{P}$ -MRS were similar to those measured in tumor-like spheroids derived from the same cell lines (22). Overestimation of the extracellular pH in the  $^{13}\text{C}$ -MRS experiments can be explained by failure of the CA-catalyzed reaction to reach isotopic equilibrium, presumably because of a lower CA activity in the colorectal tumors used here when compared to the murine lymphoma model used previously (11,12). In similar studies in the perfused ischemic rat heart, where the intracellular pH was estimated from the  $^{13}\text{CO}_2$  and  $\text{H}^{13}\text{CO}_3^-$  formed following decarboxylation of injected hyperpolarized  $^{13}\text{C}$ -pyruvate, the pH was consistently underestimated due to inhibition of CA by the ischemia-induced acidosis (23). Inhibition of CA slowed formation of  $\text{H}^{13}\text{CO}_3^-$  from the  $^{13}\text{CO}_2$  produced by decarboxylation of the injected pyruvate, slowing equilibration of the  $^{13}\text{C}$  label between the two pools, and consequent underestimation of the true pH. This problem of underestimation or overestimation of pH due to failure of the  $^{13}\text{C}$  label to equilibrate between the  $\text{H}^{13}\text{CO}_3^-$  and  $^{13}\text{CO}_2$  pools could be addressed in highly perfused organs or tumors, where there is a sufficiently high signal-to-noise ratio for the  $^{13}\text{CO}_2$  resonance, by acquiring a series of  $^{13}\text{C}$  spectra and waiting until isotope equilibration has been achieved before pH estimation. Assuming an apparent spin lattice relaxation rate ( $\rho$ ) for the hyperpolarized  $\text{H}^{13}\text{CO}_3^-$  resonance of  $0.1\text{ s}^{-1}$ , and using the measured rate of decay of the bicarbonate resonance following saturation of the  $^{13}\text{CO}_2$  resonance in the control tumors of  $0.26\text{ s}^{-1}$  ( $\rho + k$ ), then the  $t_{1/2}$  for equilibration of label between the  $\text{H}^{13}\text{CO}_3^-$  and  $^{13}\text{CO}_2$  pools would be  $\sim 4\text{ s}$ , which means that label equilibration should have been nearly complete by  $\sim 16\text{ s}$ . Measurements of cardiac pH following reperfusion were shown to reach steady state within a similar timeframe (23).

CAIX expression, which is upregulated in tumors by hypoxia, is related to a poor prognosis and a malignant phenotype and is thought to promote progression by increasing acidification of the extracellular space (5). In support of this hypothesis CAIX expression has been shown to contribute to the acidification of hypoxic cells in suspension (24). Although it has been possible to image the spatial distribution of CAIX using PET (6), it has not been possible until recently to measure directly the activity of CAIX *in vivo*. We showed previously that magnetization transfer measurements of hyperpolarized  $^{13}\text{C}$  label flux between  $\text{H}^{13}\text{CO}_3^-$  and  $^{13}\text{CO}_2$  can be used to assess the activity of the enzyme in a murine tumor model *in vivo* (11). Saturation of the  $^{13}\text{CO}_2$  resonance resulted in a decrease in the  $\text{H}^{13}\text{CO}_3^-$  peak intensity and this decrease was reduced by administration of the CA inhibitor acetazolamide. We used the technique here to measure CA activity in the two implanted human colorectal tumor models, one of which overexpressed CAIX.

The CAIX overexpressing cells showed an increase in CA activity *in vitro*, which was predominantly extracellular in location (Figure 3). This increase in CAIX expression was preserved following subcutaneous implantation of these tumor cells *in vivo*, as shown by immunohistochemical staining of excised sections of the resulting tumors (Figure 4). Surprisingly, the CA activities determined *in vivo* using  $^{13}\text{C}$  magnetization transfer measurements were inversely related to the levels of CAIX expression. Furthermore, the reduced CA activity in the CAIX overexpressing tumors was restored to control values by administration of oral bicarbonate, which has been shown previously to elevate the extracellular pH of tumors (14) (Figure 5B). The disparity between CAIX expression and activity suggests that factors other than the concentration of the protein play a dominant role in determining its activity *in vivo*.

The CA activities of the cell lines used here have been shown previously to be strongly pH-dependent *in vitro*, with inhibition at low pH and a catalytic activity that is half-maximal at a pH of approximately 6.8 (13). When the cells were grown as tumor-like spheroids, the core extracellular pH of the CAIX overexpressing spheroids was approximately 0.3 pH units lower than spheroids produced from cells transfected with the empty vector (pH 6.6 vs. 6.9) (22). The pHs measured using  $^{31}\text{P}$ -MRS in tumors derived from the same cell lines in this study, produced similar results to the experiments with spheroids (pH 6.66 vs. 6.81). Although the absolute measurements of pH made using  $^{13}\text{C}$ -MRS were artifactually high, because equilibration of hyperpolarized  $^{13}\text{C}$  label between  $\text{H}^{13}\text{CO}_3^-$  and  $^{13}\text{CO}_2$  had not reached equilibrium, the relative difference between the two groups for both spheroids and tumors was similar, with a pH difference of 0.2-0.3. These data imply that the activity expressed by CAIX in these tumors is determined predominantly by the extracellular pH rather than the concentration of the enzyme; the lower extracellular pH in the CAIX-overexpressing tumors decreasing the specific activity of the enzyme to such an extent that the activity expressed by the enzyme was less than that in the tumors with lower levels of CAIX expression. Administration of oral bicarbonate, which raised the extracellular tumor pH, restored CAIX activity in the overexpressors to levels comparable to that in the control tumors.

This study has shown, for the first time, the importance of tumor pH in regulating the activity of CA *in vivo* and provides an explanation for why CAIX may be upregulated in an hypoxic environment. The increased expression of the enzyme under these conditions compensating for a pH-dependent decrease in its specific activity. This autoregulation of CAIX activity provides a potentially important mechanism to prevent excessive extracellular acidosis and supports the

observation that CAIX has other roles in metastasis (25). These experiments further suggest that the measured CA activity could be used as a surrogate measure of extracellular pH in situations where the  $^{13}\text{CO}_2$  is below the limits of detection, which may be relevant in future human studies (26).

Other isoforms may also contribute to the CA activity measured here *in vivo* using hyperpolarized  $\text{H}^{13}\text{CO}_3^-$ . Previous work has shown reciprocal regulation of CAIX and CAXII expression, however this effect is very small (13), and is unlikely to account for the paradoxical effect we have observed here, where increased CAIX expression was accompanied by a decrease in measured activity *in vivo*. Furthermore, measurements of  $\text{CO}_2$  hydration *in vitro* have shown a higher membrane-bound CA activity in a CAIX overexpressing cell line compared to empty vector cells (13), which indicates that any increase in CAIX activity is not compensated for by a decrease in CAXII expression.

Blood carbonic anhydrase may also contribute to total CA activity measured *in vivo*. Although the vascular volume of the tumor is relatively small we expect much of the injected hyperpolarized  $\text{H}^{13}\text{CO}_3^-$  to be present initially in the vascular compartment. However, the effects of blood carbonic anhydrase activity and vascular bicarbonate on the measured pH and CA activity are evidently small since neither can explain the tumor acidification following CAIX overexpression, observed with both 3-APP and hyperpolarized  $\text{H}^{13}\text{CO}_3^-$ , or the decrease in measured CA activity following CAIX overexpression. The increased expression of the enzyme under acidic conditions could thus compensate for a pH-dependent decrease in its specific activity. This occurs despite the fact that the proteoglycan domain present in CAIX confers upon it a more acidic pH optimum than other isoforms. A plot of  $k_{\text{cat}}/K_m$  for the

hydration of CO<sub>2</sub> catalyzed by CAIX gives an apparent pKa of 6.5, as compared to 6.9 – 7.1 for some of the other isoforms (27). Interestingly this domain is also involved in cell adhesion and tumor invasion processes (5,28).

Changes in the unlabeled endogenous bicarbonate pool may affect the observed enzyme catalyzed exchange between hyperpolarized H<sup>13</sup>CO<sub>3</sub><sup>-</sup> and <sup>13</sup>CO<sub>2</sub> because of competition between labeled and unlabeled bicarbonate for the enzyme. Note that the CO<sub>2</sub> pool is not relevant since the magnetization in this pool is destroyed by selective irradiation. An increase in pH would be expected to increase the unlabeled bicarbonate pool and therefore decrease the measured enzyme catalyzed flux of label between H<sup>13</sup>CO<sub>3</sub><sup>-</sup> and <sup>13</sup>CO<sub>2</sub>. However, we have demonstrated the opposite, with an increase in measured enzyme activity at higher pH. We have also shown that administration of oral bicarbonate (which will increase the levels of unlabeled bicarbonate) increases the measured CA activity. Therefore any changes in unlabeled endogenous bicarbonate concentration as a result of changes in pH cannot explain the results shown here.

On some occasions two peaks were observed in the region of the bicarbonate peak approximately 1 ppm apart (as shown in a separate experiment in Figure 5C). When present, the downfield peak did not decrease following saturation of the <sup>13</sup>CO<sub>2</sub> resonance, indicating that it was either not in exchange with CO<sub>2</sub> or only in very slow exchange on the time scale of the polarization life-time. This peak is likely to represent a bound form of <sup>13</sup>CO<sub>2</sub> e.g. a carbamate formed from the reaction of an amine with the <sup>13</sup>CO<sub>2</sub>. Carbamylated hemoglobin groups have previously been described within a few ppm of the H<sup>13</sup>CO<sub>3</sub><sup>-</sup> signal in <sup>13</sup>C-MR spectra and the extra peak demonstrated in these experiments may represent this or other

carbamate compounds (29). The shift could represent compartmentalization of the  $\text{H}^{13}\text{CO}_3^-$  signal but appears to be too large to be explained by differences in hydrogen bonding of bicarbonate in the intra- and extracellular compartments (30). Irrespective of the origin of the downfield resonance, it will not contribute to the measured pH given the lack of exchange with the  $\text{CO}_2$  pool, and was therefore excluded from the measurements of pH.

In conclusion, we have shown that measurements of pH derived from the ratio of the peak intensities of  $\text{H}^{13}\text{CO}_3^-$  and  $^{13}\text{CO}_2$ , following injection of hyperpolarized  $\text{H}^{13}\text{CO}_3^-$  can be overestimated if equilibration of  $^{13}\text{C}$  label is slow on the timescale of the  $^{13}\text{C}$ -MRS measurements; in the models used here equilibration was estimated to have been achieved by ~16 s.  $^{13}\text{C}$ -MRS magnetization transfer measurements of CA activity *in vivo* demonstrated a disparity between expression of the CAIX isoform and overall CA activity, which can be explained by the pH-dependence of the enzyme. These measurements of CA activity suggest that CAIX expression is increased by hypoxia in order to compensate for the decreased specific activity of the enzyme resulting from the lower pH, and support the hypothesis that a major function of CAIX is to promote an acidic extracellular environment.



## **Acknowledgments**

The authors acknowledge funding support from Cancer Research UK (CRUK; C19212/A16628; C19212/A911376), the National Institute for Health Research Cambridge Biomedical Research Centre and the School of Clinical Medicine at the University of Cambridge, the CRUK and Engineering and Physical Sciences Research Council (EPSRC) Cancer Imaging Centre in Cambridge and Manchester. E.M.S. is a recipient of funding from the European Union Seventh Framework Programme (FP7/2007-2013) under the Marie Curie Initial Training Network METAFLUX and has support from the Calouste Gulbenkian Foundation, Champalimaud Foundation, Ministerio de Saude and Fundacao para a Ciencia e Tecnologia, Portugal. The authors would like to thank Dr Dominick McIntyre and the staff in Cancer Research UK Cambridge Institute animal facility for their assistance with experiments.

## References

1. Swietach P, Hulikova A, Vaughan-Jones RD, Harris AL. New insights into the physiological role of carbonic anhydrase IX in tumour pH regulation. *Oncogene* 2010;29(50):6509-21.
2. Warburg O. On the origin of cancer cells. *Science* 1956;123(3191):309-14.
3. Newell K, Franchi A, Pouyssegur J, Tannock I. Studies with glycolysis-deficient cells suggest that production of lactic acid is not the only cause of tumor acidity. *Proc Natl Acad Sci U S A* 1993;90(3):1127-31.
4. Wykoff CC, Beasley NJ, Watson PH, Turner KJ, Pastorek J, Sibtain A, et al. Hypoxia-inducible expression of tumor-associated carbonic anhydrases. *Cancer Res* 2000;60(24):7075-83.
5. Potter CP, Harris AL. Diagnostic, prognostic and therapeutic implications of carbonic anhydrases in cancer. *Br J Cancer* 2003;89(1):2-7.
6. Divgi CR, Pandit-Taskar N, Jungbluth AA, Reuter VE, Gonen M, Ruan S, et al. Preoperative characterisation of clear-cell renal carcinoma using iodine-124-labelled antibody chimeric G250 (<sup>124</sup>I-cG250) and PET in patients with renal masses: a phase I trial. *Lancet Oncol* 2007;8(4):304-10.
7. Ardenkjaer-Larsen JH, Fridlund B, Gram A, Hansson G, Hansson L, Lerche MH, et al. Increase in signal-to-noise ratio of > 10,000 times in liquid-state NMR. *Proc Natl Acad Sci U S A* 2003;100(18):10158-63.
8. Gallagher FA, Kettunen MI, Brindle KM. Biomedical applications of hyperpolarized <sup>13</sup>C magnetic resonance imaging. *Prog in NMR Spect* 2009;55(4):285-95.
9. Kurhanewicz J, Vigneron DB, Brindle K, Chekmenev EY, Comment A, Cunningham CH, et al. Analysis of cancer metabolism by imaging hyperpolarized nuclei: prospects for translation to clinical research. *Neoplasia* 2011;13(2):81-97.
10. Brindle KM, Bohndiek SE, Gallagher FA, Kettunen MI. Tumor imaging using hyperpolarized <sup>13</sup>C magnetic resonance spectroscopy. *Mag Reson Med* 2011;66(2):505-19.
11. Gallagher FA, Kettunen MI, Day SE, Hu DE, Ardenkjaer-Larsen JH, Zandt R, et al. Magnetic resonance imaging of pH in vivo using hyperpolarized <sup>13</sup>C-labelled bicarbonate. *Nature* 2008;453(7197):940-3.
12. Gallagher FA, Kettunen MI, Brindle KM. Imaging pH with hyperpolarized <sup>13</sup>C. *NMR Biomed* 2011;24(8):1006-15.
13. McIntyre A, Patiar S, Wigfield S, Li JL, Ledaki I, Turley H, et al. Carbonic anhydrase IX promotes tumor growth and necrosis in vivo and inhibition enhances anti-VEGF therapy. *Clin Cancer Res* 2012;18(11):3100-11.
14. Raghunand N, He X, van Sluis R, Mahoney B, Baggett B, Taylor CW, et al. Enhancement of chemotherapy by manipulation of tumour pH. *Br J Cancer* 1999;80(7):1005-11.
15. Gillies RJ, Liu Z, Bhujwala Z. <sup>31</sup>P-MRS measurements of extracellular pH of tumors using 3-aminopropylphosphonate. *The American journal of physiology* 1994;267:C195-203.
16. Schabel MC, Parker DL. Uncertainty and bias in contrast concentration measurements using spoiled gradient echo pulse sequences. *Physics in medicine and biology* 2008;53(9):2345-73.

17. Priest AN, Gill AB, Kataoka M, McLean MA, Joubert I, Graves MJ, et al. Dynamic contrast-enhanced MRI in ovarian cancer: Initial experience at 3 Tesla in primary and metastatic disease. *Magn Reson Med* 2010;63(4):1044-9.
18. Korkeila E, Talvinen K, Jaakkola PM, Minn H, Syrjanen K, Sundstrom J, et al. Expression of carbonic anhydrase IX suggests poor outcome in rectal cancer. *Br J Cancer* 2009;100(6):874-80.
19. Booth TC, Kettunen MI, Gallagher FA, Kennedy BW, Rodrigues TB, Bohndiek SE, et al. Determination of the pKa of a hyperpolarized H<sup>13</sup>CO<sub>3</sub><sup>-</sup> pH probe. *Proc Intl Soc Mag Reson Med* 2012; Melbourne, Australia. p 1671.
20. Gillies RJ, Raghunand N, Garcia-Martin ML, Gatenby RA. pH imaging. A review of pH measurement methods and applications in cancers. *IEEE engineering in medicine and biology magazine : the quarterly magazine of the Engineering in Medicine & Biology Society* 2004;23(5):57-64.
21. Stubbs M, Bhujwala ZM, Tozer GM, Rodrigues LM, Maxwell RJ, Morgan R, et al. An assessment of <sup>31</sup>P MRS as a method of measuring pH in rat tumours. *NMR Biomed* 1992;5(6):351-9.
22. Swietach P, Patiar S, Supuran CT, Harris AL, Vaughan-Jones RD. The role of carbonic anhydrase 9 in regulating extracellular and intracellular pH in three-dimensional tumor cell growths. *J Biol Chem* 2009;284(30):20299-310.
23. Schroeder MA, Swietach P, Atherton HJ, Gallagher FA, Lee P, Radda GK, et al. Measuring intracellular pH in the heart using hyperpolarized carbon dioxide and bicarbonate: a <sup>13</sup>C and <sup>31</sup>P magnetic resonance spectroscopy study. *Cardiovasc Res* 2010;86(1):82-91.
24. Svastova E, Hulikova A, Rafajova M, Zat'ovicova M, Gibadulinova A, Casini A, et al. Hypoxia activates the capacity of tumor-associated carbonic anhydrase IX to acidify extracellular pH. *FEBS Lett* 2004;577(3):439-45.
25. Gieling RG, Williams KJ. Carbonic anhydrase IX as a target for metastatic disease. *Bioorg Med Chem* 2013;21(6):1470-6.
26. Nelson SJ, Kurhanewicz J, Vigneron DB, Larson PE, Harzstark AL, Ferrone M, et al. Metabolic imaging of patients with prostate cancer using hyperpolarized [1-<sup>13</sup>C]pyruvate. *Sci Transl Med* 2013;5(198):198ra08.
27. Innocenti A, Pastorekova S, Pastorek J, Scozzafava A, De Simone G, Supuran CT. The proteoglycan region of the tumor-associated carbonic anhydrase isoform IX acts as an intrinsic buffer optimizing CO<sub>2</sub> hydration at acidic pH values characteristic of solid tumors. *Bioorganic & medicinal chemistry letters* 2009;19(20):5825-8.
28. Svastova E, Zilka N, Zat'ovicova M, Gibadulinova A, Ciampor F, Pastorek J, et al. Carbonic anhydrase IX reduces E-cadherin-mediated adhesion of MDCK cells via interaction with beta-catenin. *Experimental cell research* 2003;290(2):332-45.
29. Morrow JS, Matthew JB, Wittebort RJ, Gurd FR. Carbon 13 resonances of <sup>13</sup>CO<sub>2</sub> carbamino adducts of alpha and beta chains in human adult hemoglobin. *J Biol Chem* 1976;251(2):477-84.
30. Himmelreich U, Drew KN, Serianni AS, Kuchel PW. <sup>13</sup>C NMR studies of vitamin C transport and its redox cycling in human erythrocytes. *Biochemistry* 1998;37(20):7578-88.

## **Figure legends**

**Figure 1.** Measurements of CA activity *in vitro*. **A:** EPI image of  $\text{H}^{13}\text{CO}_3^-$  immediately following the addition of hyperpolarized  $\text{H}^{13}\text{CO}_3^-$ . The gray scale is shown next to the image. **B:** A similar EPI image after 670 ms saturation of the  $^{13}\text{CO}_2$  resonance. **C:** CA activity map: the ratio of image A over image B. Noise has been reduced as described in the methods; the brighter the image, the higher the CA activity. The concentration of CA ( $\mu\text{g}/\text{ml}$ ) is shown adjacent to each tube. **D:** Plot of the slope of the natural logarithm of the relative  $\text{H}^{13}\text{CO}_3^-$  signal intensity in each tube over time and the corresponding concentration of CA ( $n = 5$ ).

**Figure 2.** Western blot showing overexpression of CAIX in the CA9/1 cell line compared to the wild-type HCT116 cells and cell line (EV5) that had been transfected with the empty vector. Actin, at 42 kDa, was used as a loading control.

**Figure 3.** Measurements of CA activity, normalized to protein content, in CAIX overexpressing cells (CA9/1) and control cells (EV5) and in lysed cell extracts; average  $\pm$  standard error; \*\*\*  $p < 0.005$ ;  $n$  values shown in each case.

**Figure 4.** Immunohistochemical staining for CAIX expression in representative sections from murine tumor xenografts. H&E and CAIX stained slides are shown from three tumor types. **A:** wild-type HCT116; **B:** CAIX overexpressing cells (CA9/1); **C:** control cells (EV5). **i:** H&E of whole tumor slices; **ii:** CAIX staining of the same slices; **iii:** CAIX staining of a representative portion of each tumor at x20 magnification (scale bar demonstrated).

**Figure 5. A:** Representative spectrum acquired from a CA9/1 tumor following tail vein injection of hyperpolarized  $\text{H}^{13}\text{CO}_3^-$ , showing  $\text{H}^{13}\text{CO}_3^-$  and  $^{13}\text{CO}_2$  resonances at 161 and 125 ppm respectively. **B:** Magnetization transfer measurements of tumor CA activity showing a decrease in hyperpolarized  $\text{H}^{13}\text{CO}_3^-$  signal intensity following saturation of the  $^{13}\text{CO}_2$  resonance. Results from three animal groups are shown: CAIX over expressing tumors (solid line; CA9/1), control tumors with low expression of CAIX (dashed line; EV5) and the CAIX over expressing line following the administration of bicarbonate in the drinking water, which elevated the tumor pH (dotted line; CA9/1 +  $\text{HCO}_3^-$ ). The number of animals in each case is indicated in parentheses. **C:** Two resonances were observed in the  $\text{H}^{13}\text{CO}_3^-$  region of the spectrum in some cases. The plot shows a series of spectra acquired every 1 s following the injection of hyperpolarized  $\text{H}^{13}\text{CO}_3^-$  to demonstrate this. The upfield resonance decayed rapidly following saturation of the  $^{13}\text{CO}_2$  resonance, which commenced 10 s after  $\text{H}^{13}\text{CO}_3^-$  injection (arrowed).